Phonon properties of Si and BN crystals

Lovro Anto Barišić*
Prirodoslovno - matematički fakultet, Fizički odsjek, Bijenička 32, Zagreb and
Mentor : dr. sc. Vito Despoja, Institut za fiziku, Zagreb
(Dated: January 25, 2022)

The phonon spectra of silicon Si and boron nitride (BN) crystals are calculated using Quantum ESPRESSO. The primitive cell of the Si diamond like crystals involve two atoms, corresponding to two TO and two TA modes, and one LO and LA mode. At Γ point the optical modes are degenerate. The diamond like cubic zinc-blende structure of the BN involves two atoms as in the Si case, one B and one N atom with similar masses. Therefore, resemblances with silicon may be expected in the phonon spectrum. However, one fundamental difference appears, at Γ point a strong TO-LO splitting is clearly observed. This is a direct consequence of the polar nature of BN crystals, causing long-range forces for LO vibrations, which notably complicate calculations. The hexagonal graphite like BN structure is characterized by the van der Waals interactions between the layers. Because of these weak bonds between the layers, at Γ point one observes that some of the optical modes have notably lower frequencies than the others.

I. CRYSTAL PROPERTIES

We have applied DFT calculations, using Quantum ESPRESSO, to find the dynamical matrixes $\mathcal{D}_{s\alpha,s\prime\alpha\prime}(\vec{q})$ that describe the lattice (phonon) dynamics for a given wavevector $\vec{q}$. Here, s and $s\prime$ denote different atoms in the primitive cell, whereas α and $\alpha\prime$ denote different directions of atomic motion. Crystal properties of the silicon and boron nitride (BN) in the cubic zinc-blende (diamond like) structure, cBN, and, hexagonal (graphite like), hBN, structure are obtained in this way.

Since the two crystals, silicon and cBN, share similar properties, having the diamond like structure, our goal is to study differences between these two systems. We are particularly interested in the appearance of the LO-TO splitting, discussing the interesting question of why this splitting is observed experimentally for the BN crystals and not for the silicon crystals.

I.1. DFT calculation

In the first step, the crystallographic structure needs to be determined. This step then provides the input file for the SCF calculations. The lattice parameters for each of the crystals are obtained by looking for the minimal ground state energy. This minimal energy defines the equilibrium positions of atoms within the crystal structure, while phonon excitations represent the harmonic oscillations of the lattice around this equilibrium position.

The dynamical matrix $\mathcal{D}_{s\alpha,s\prime\alpha\prime}(\vec{q})$ describes the phonon dynamics for a given wavevector $\vec{q}$. For example, in the case of cBN, they are two atoms s and $s\prime$ in the primitive cell. The motion of these atoms involves all the three dimensions, with α and $\alpha\prime$ representing these different degrees of freedom of each atom.

For the BN zinc-blende structure, our procedure gives the value of a =6.74 a.u. for the distances between atoms. This value is only slightly different from the experimentally observed value, which is according Ref. [1] a =6.83 a. u. In the same way, we find a =10.2 a.u. for the silicon diamond like cubic structure, and 4.746 a.u. for the hexagonal boron nitride hBN.

I.2. Dynamical matrix for Si and BN crystals at $\vec{q} = 0$

For $\vec{q} = 0$, the phonon is described by a stationary wave for which the atoms in all the unit cell oscillate in phase. The analysis of the dynamical matrix, which in general depend of all three components of the phonon momentum $\vec{q}$, can be simplified for $\vec{q} = 0$ by discussing vibrations in a particular direction. For a direction, let say $\vec{z}$, we can consider the equations of motion for the displacements of the two atoms v_1 and v_2. The corresponding eigenvalue problem is given by

$$\begin{bmatrix} (\mathcal{C}_z)_{11} & (\mathcal{C}_z)_{12} \\ (\mathcal{C}_z)_{21} & (\mathcal{C}_z)_{22} \end{bmatrix} \begin{bmatrix} v_1 \\ v_2 \end{bmatrix} = \omega^2 \begin{bmatrix} m_1 v_1 \\ m_2 v_2 \end{bmatrix} \tag{1}$$

The first useful property of the interatomic force constants C for the analysis of the solutions follows from the translational symmetry: $(\mathcal{C}_z)_{ij} = \frac{\partial^2 \epsilon}{\partial v_i \partial v_j} = \frac{\partial^2 \epsilon}{\partial v_2 \partial v_1} = (\mathcal{C}_z)_{12}$. In other words, the matrix in Eq. (2) is symmetric. The dynamical matrix is obtained from the interatomic force constants by the substitution,

$$D(\vec{q})_{ij} = \frac{1}{\sqrt{M_i M_j}} C(\vec{q})_{ij}$$

The second useful property follows from physical expectations for vanishing momenta. Namely, it is well known that the energy of all acoustic phonon excitations, irrespectively of the direction and polarization, vanishes

* lovro.anto.barisic@gmail.com

at $\vec{q} = 0$. Therefore, one of the eigenvalues given by Eq. (2) should be zero for the acoustic motion of the two atoms within the unit cell. Thus, the eiqenvalue problem in Eq. (2) reduces to the following form:

$$\begin{bmatrix} (\mathcal{C}_z)_{11} & -a \\ -a & (\mathcal{C}_z)_{22} \end{bmatrix} \begin{bmatrix} v \\ v \end{bmatrix} = 0$$

where the displacement v is arbitrary. Consequently, one obtains that

$$\begin{bmatrix} (\mathcal{C}_z)_{11} & (\mathcal{C}_z)_{12} \\ (\mathcal{C}_z)_{21} & (\mathcal{C}_z)_{22} \end{bmatrix} = \begin{bmatrix} a & -a \\ -a & a \end{bmatrix} \tag{2}$$

where the sign of nondiagonal matrix elements is related to the fact that the restoring force for the translation of the whole crystal vanishes.

The properties of the dynamical matrix $\mathcal{D}_{s\alpha,s\prime\alpha\prime}(\vec{q}=0)$ at $\vec{q}=0$ are well recognized by Quantum ESPRESSO for silicon, for which one obtains all the matrix elements to be the same. For the BN calculations, one obtains the values of the matrix elements that are very close to each other:

$$\begin{bmatrix} (\mathcal{C}_z)_{11} & (\mathcal{C}_z)_{12} \\ (\mathcal{C}_z)_{21} & (\mathcal{C}_z)_{22} \end{bmatrix}_{BN} = \begin{bmatrix} 0.52144 & -0.52110 \\ -0.52111 & 0.52280 \end{bmatrix} \tag{3}$$

While we know that the acoustic modes has the zero energy at the Γ point, we may now calculate in addition the frequency of the degenerate optical modes, obtaining 1062 cm^{-1}. This value is very close to the frequency obtained by the DFT calculation 1078 cm^{-1}.

As our next step, we are interested in the phonon frequency behaviors when we take the limit $\vec{q} \to 0$. Again, we use Quantum ESPRESSO to calculate the dynamical matrix for $\alpha = \alpha\prime = z$. For silicon, and approximately for BN, we observe that the acoustic frequency increases linearly with $\vec{q}$ near the Γ point, as shown in Fig. 1 and Fig. 2 for the silicon and the cBN, respectively. The results in Fig. 2 are in very god agreement with Ref. [7]. Similarly, the results for the silicon agree with Refs. [8, 9].

For silicon, we observe from Fig. 1 that the calculations of the optical mode give the same value in the $\vec{q} \to 0$ limit as for the $\vec{q}=0$ point. Furthermore, the two optical modes are degenerated at $\vec{q}=0$. For BN in Fig. 2), there are some discrepancies. Namely, in this case, we see a gap opening for $\vec{q}=0$. In particular, there is a jump in the dispersion from 1075 cm^{-1} to 1307 cm^{-1} in Fig. 2, which may be seen by comparing the frequency of the first blue triangle with others. Our next task is therefore to analyze this behavior, which is related to the existence of the long-range polar forces in BN and the LO-TO splitting. This effect is not present for silicon crystals since there are no such long-range forces in these crystals.

II. LO-TO SPLITTING

We are interested in the dispersions of the LO and the TO phonons near the Γ point in systems with long-range forces. In particular, the origin of the LO-TO splitting in polar materials is caused by the presence of the macroscopic polarization density, generated by the atomic displacement $\vec{v}_{LO}$ and the associated electric fields [11].

II.1. Theoretical background

We may write the Fourier transform of the polarization density in the form given by

$$\vec{P}(\vec{q}) = \frac{e^2}{\Omega} \sum_{n=0} \mathcal{Z}_n \cdot \vec{v}_{LO} \tag{4}$$

Here, e is the elementary charge and Ω is the volume of the $3D$ unit cell (or the surface for the $2D$ unit cell). We also introduce the tensor of the Born effective charges $\mathcal{Z}_n$, associated with the atom n within the unit cell. If we consider long-wavelength vibrations of the LO and TO modes, we observe that they are quite mechanically similar [11]. On the other hand, if the material is polar, the LO modes may generate long-range fields that make them different from TO modes.

Using the Maxwell equations one obtains the following expressions for macroscopic (averaged) fields in the absence of free charges,

$$\vec{\nabla}\vec{D} = 0 \quad \Rightarrow \quad \vec{q}\vec{D}_q = 0 \tag{5}$$

$$\vec{\nabla} \times \vec{E} = 0 \quad \Rightarrow \quad \vec{q} \times \vec{E}_q = 0 \tag{6}$$

We see that for longitudinal fields, $\vec{D}_q \parallel \vec{q}$, D_q should vanish, $\vec{D}_q = 0 = \vec{E}_q + 4\pi\vec{P}_q$. Thus, the LO modes, which induce an average polarization charge density $\vec{P}$, generate a macroscopic electric field $\vec{E}$, parallel to the phonon momentum $\vec{q}$. On the other hand, for transverse fields, $\vec{q} \perp \vec{E}, \vec{P}$, Eq. (6) gives $\vec{E} = 0$, which means that there are no macroscopic fields. This is the case of the electric field associated to the TO vibrations, which is orthogonal to the direction of the phonon momentum $\vec{q}$.

The Born effective charge describes the atomic response to macroscopic field, generating a force opposing the LO vibration. This effect increases the energy cost of the displacement for the LO modes in comparison to the energy needed for the TO modes displacement. Following the analysis given in Ref. [3], one may derive the relation:

$$\omega_{LO}^2 = \omega_{TO}^2 + \mathcal{W}_c(\vec{q}) \frac{e^2|\vec{q}|^2}{\Omega} \left(\sum_n \frac{\vec{e}\vec{q} \cdot \mathcal{Z}_n \cdot \vec{e}_{LO}^n}{M_n} \right)^2 \tag{7}$$

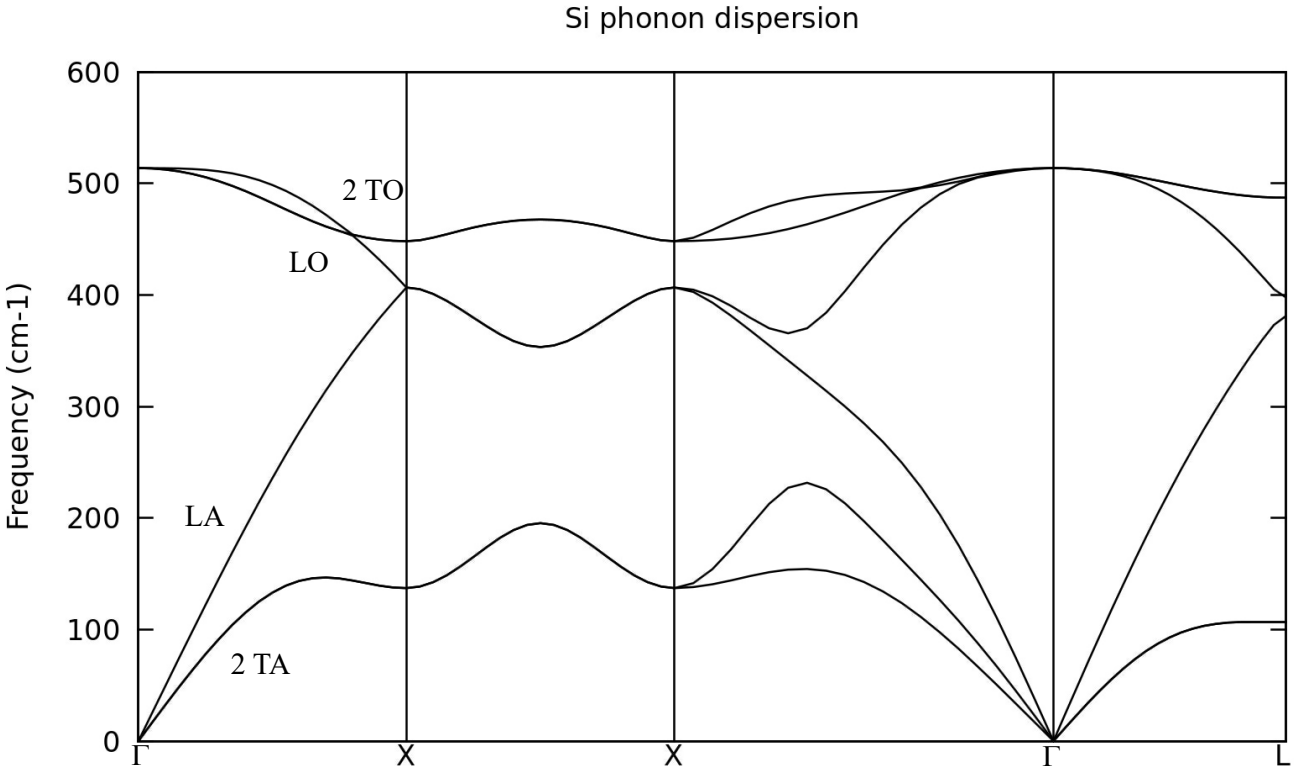

Figure 1. Phonon dispersion of for silicon along $\Gamma \to X \to X \to \Gamma \to L$ crystal symmetry lines. As the unit cell involves two atoms, we expect six different frequencies of vibrations for a given momentum $\vec{q}$: the three acoustic and the three optical modes. We see in Γ point, corresponding to $\vec{q} = 0$, that all the acoustic frequencies and all the optical frequencies are degenerated. As we move in the reciprocal lattice space, the q_x, q_y and q_z dispersions are no longer equivalent and the phonon modes lose their degeneracy.

In analogy to Eq. (7), it is possible to derive the corresponding relation for the dynamical matrix,

$$\mathcal{D}_{s\alpha,s\prime\alpha\prime}(\vec{q}\to 0) = \mathcal{D}_{s\alpha,s\prime\alpha\prime}(\vec{q}=0) + \mathcal{W}_c(\vec{q})\frac{4\pi e^2}{\Omega}\left(\frac{(\vec{\mathcal{Z}}_{s\alpha}\cdot\vec{q})(\vec{\mathcal{Z}}_{s\prime\alpha\prime}\cdot\vec{q})}{\vec{q}\cdot\hat{\epsilon}\cdot\vec{q}}\right)^2 \quad (8)$$

Here, $\hat{\epsilon}$ is the dielectric tensor, which can also be calculated by the DFT calculations.

Using Eq. (8), we may now check the consistency of the DFT calculations. In particular, for $\vec{q} = 0$, the dielectric tensor and the effective charge are obtained as

$$\hat{\epsilon} = \begin{bmatrix} 4.538 & 0 & 0 \\ 0 & 4.538 & 0 \\ 0 & 0 & 4.538 \end{bmatrix} \quad (9)$$

$$\vec{\mathcal{Z}}_B = -\vec{\mathcal{Z}}_N = \begin{bmatrix} 1.864 & 0 & 0 \\ 0 & 1.864 & 0 \\ 0 & 0 & 1.864 \end{bmatrix} \quad (10)$$

Using the properties of the dynamical matrix discussed in Sec. I.2 and taking the average value of the matrix elements for a in Eq. (2), one obtains the results in the first column in Table I. The results obtained directly by Quantum ESPRESSO are given by the second column in the Table I.

	average m.e.	QE
$\mathcal{D}_{s\alpha,s\prime\alpha\prime}(\vec{q}=0)$	1062 cm^{-1}	1078 cm^{-1}
$\mathcal{D}_{s\alpha,s\prime\alpha\prime}(\vec{q}\to 0)$	1290 cm^{-1}	1307 cm^{-1}

Table I. Comparison of the estimate obtained by enforcing the symmetry of the dynamical matrix and the direct Quantum ESPRESSO (QE) results.

We see that the differences in Table I are within a reasonable range.

II.2. Interpolation scheme

Since it is time consuming and computer demanding to calculate the dynamical matrix $\mathcal{D}_{s\alpha,s\prime\alpha\prime}(\vec{q})$, it is convenient to calculate this matrix for a set of momenta $\vec{q}$ and to use the interpolation scheme to calculate $\mathcal{D}_{s\alpha,s\prime\alpha\prime}(\vec{q})$ for other momenta $\vec{q}$. The main idea behind

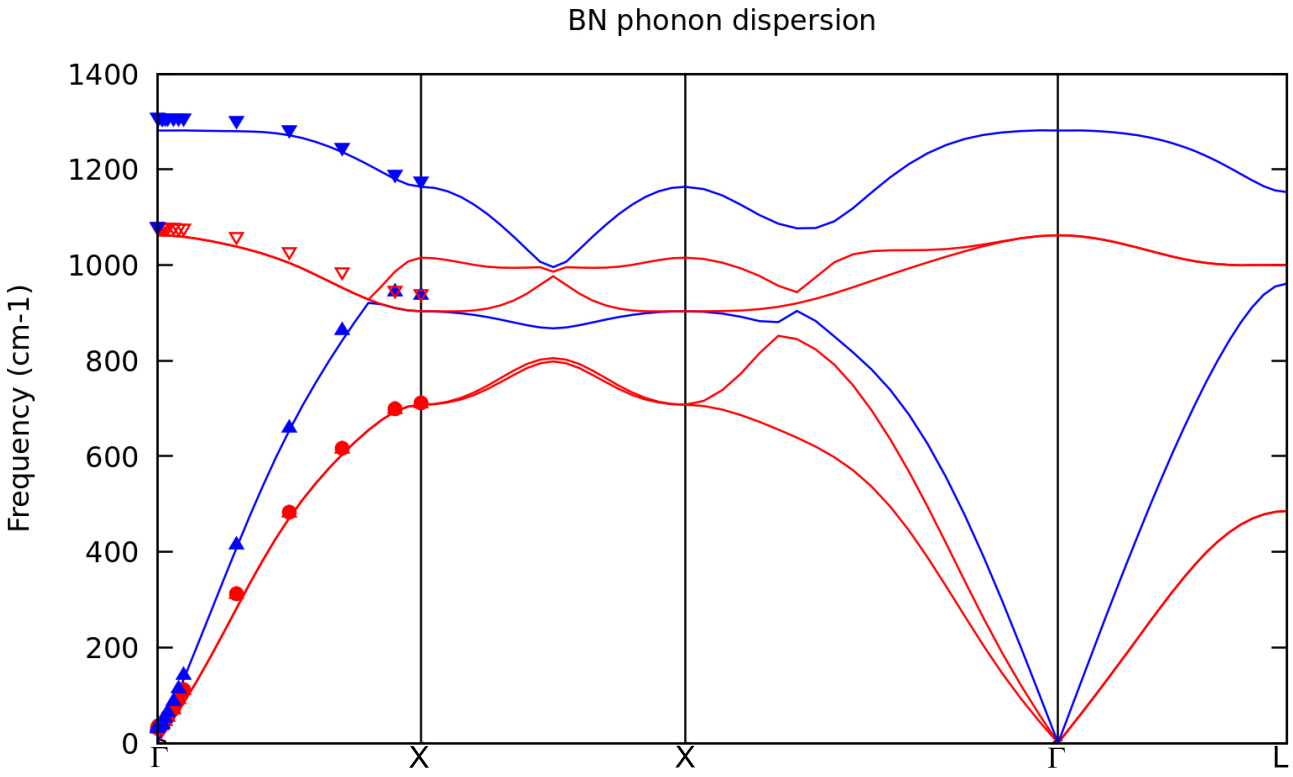

Figure 2. Phonon dispersion of the cubic zinc-blende BN between $\Gamma \to X \to X \to \Gamma \to L$ points. The red color denotes for TO modes while the blue lines are for the LO modes. As the unit cell used in the calculation has two atoms B and N we expect six different frequencies of vibrations, the three acoustic and the three optical. We see in Γ point that all the acoustic frequencies are degenerate while the optical frequencies have a gap between the TO (in red) and LO (in blue) frequencies. The continuous lines are obtained using Fourier interpolation of the phonon dispersion, while the results denoted by symbols are obtained by direct calculation.

this approach is that the exact dynamical matrix change smoothly in $\vec{q}$ space.

That is, in the first step, one needs to calculate the dynamical matrix for a representative, yet finite set of $\vec{q}$ points on the grid in the reciprocal space of the crystal. In the next step, the Fourier transform is taken to calculate the dynamical matrix as a function of the continuous real space variable $\vec{R}$,

$$F(\vec{R}) = \sum_{\vec{q} \in grid} D(\vec{q}) e^{i\vec{q}\vec{R}} \, .$$

In the final step, the dynamical matrix is taken back into the reciprocal space, assuming that it is well defined for any values of the wavevector $\vec{q}$,

$$\tilde{D}(\vec{q}) = \frac{1}{N} \sum_{\vec{R}} F(\vec{R}) e^{-i\vec{q}\vec{R}}$$

Using this particular procedure within Quantum ESPRESSO, the phonon dispersion of silicon is obtained, as shown in Fig. 1.

II.3. Phonon dispersion along the crystal symmetry axis

The problem of modeling crystals that are characterized by the LO-TO splitting is that their dynamical matrix, besides the smooth analytical part, involve a non-analytic part as well. The latter may change rapidly and become singular as the symmetry point is approached, $\vec{q} \to 0$. Such a kind of behavior we observe in the modeling of the cubic zinc-blende BN structure. In particular, following Ref. [2] (Eq. (73)), the non-analytic part of the dynamical matrix in a polarizable crystal can be described by the following term:

$$\tilde{N}(\vec{q})_{\beta s \beta' s'} = \sum_{\vec{G} \neq 0} \frac{4\pi}{\Omega} \frac{(q+G)_\alpha Z_{\alpha,\beta s} (q+G)_{\alpha'} Z_{\alpha',\beta' s'}}{(q+G)_\alpha \epsilon_{\alpha\alpha'} (q+G)_{\alpha'}} \quad (11)$$

where we sum over G involves the summation over the reciprocal lattice vectors $\vec{G}$. In practice, one sums over a finite number of vectors of the reciprocal lattice, with the precision of calculations of $\tilde{N}(\vec{q})_{\beta s \beta' s'}$ that increases with the number of vectors taken. In Eq. (11), Ω is the volume of the system defined by the total number of reciprocal

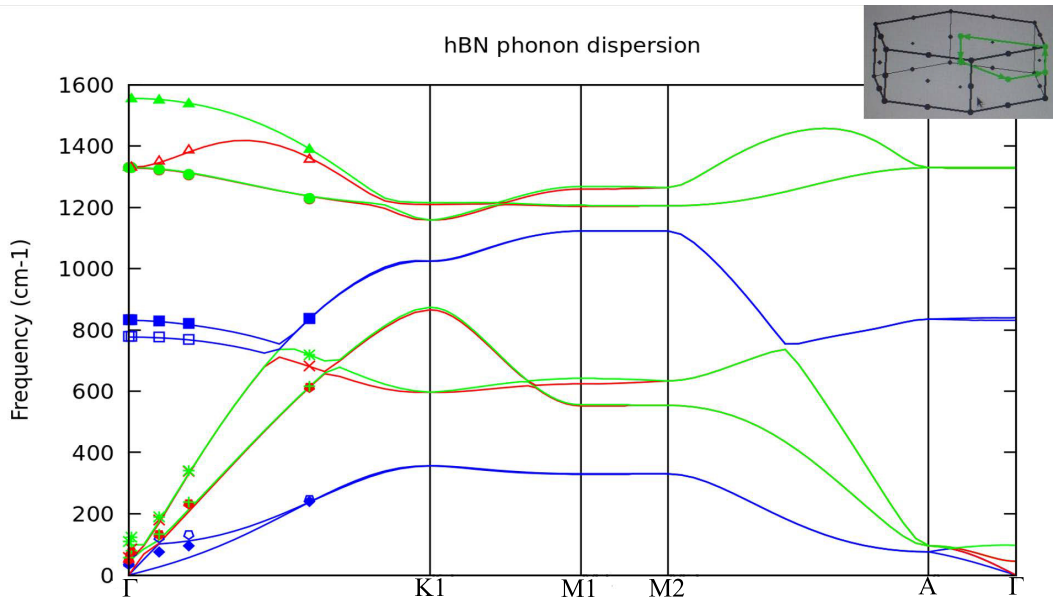

Figure 3. Phonon dispersion of hBN along the crystal symmetry lines $\Gamma \to K1 \to M1 \to M2 \to A \to \Gamma$. The red and the green color is used for the in-plane modes at Γ point, while the blue curves correspond to the out of plane z modes. Depending on the direction in the Brillouin zone, we can clearly see the LO-TO splitting for the in-plane modes, particularly near the Γ point. The other interesting result is the splitting of the two z optical modes along the lines in the plane. However, for the lines in the z direction, the two modes collapse on each other. Since the unit cell in our calculations involves four atoms: two B and two N atoms, there are twelve different frequencies of vibrations, corresponding to the six acoustic and the six optical modes. The continuous curves are obtained using Fourier interpolation, while the triangles are the $\vec{q}$ points obtained by the direct calculations.

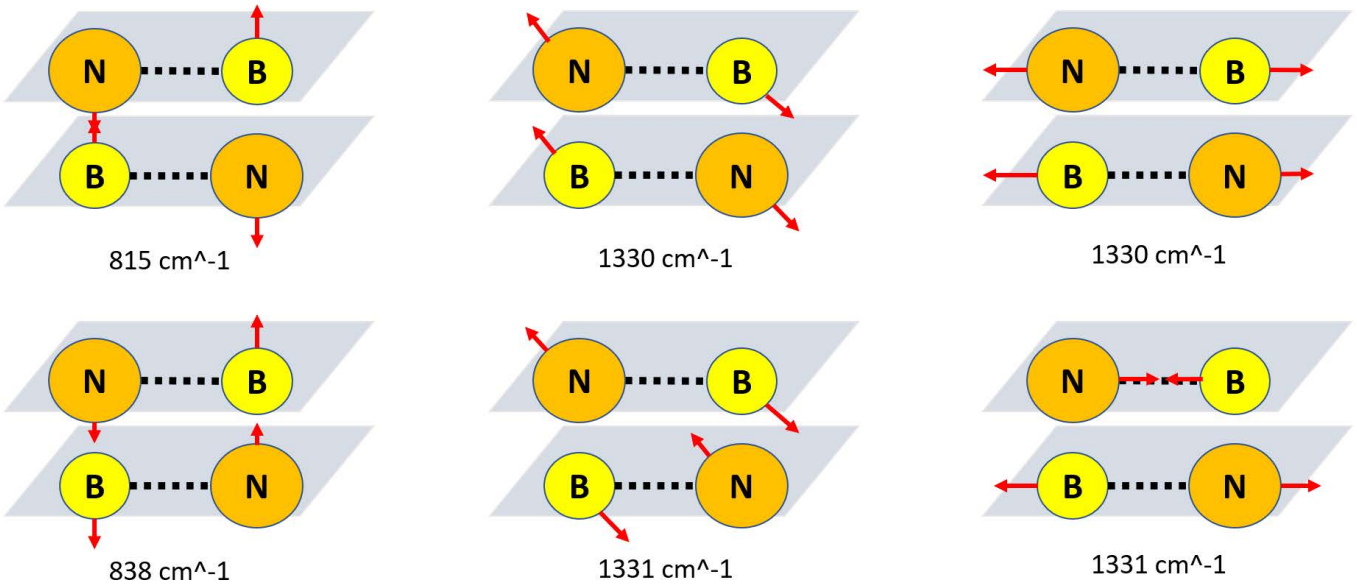

Figure 4. Representation of the six optical modes for $\vec{q} = 0$ within one unit cell of the hBN crystal. For each of the modes, the frequency of the phonon vibration is provided as well.

lattice vectors taken into account, whereas $\epsilon_{\alpha\alpha\prime}$ is the dielectric tensor and $Z_{\alpha,\beta s}$ is the effective charge.

In modeling, the non-analytic part is usually treated separately from the analytical part. That is, once that the dynamical matrix for the polar crystal is obtained for a finite number of $\vec{q}$ points on the grid in the reciprocal space, $\mathcal{D}_{s\alpha,s\prime\alpha\prime}(\vec{q})$, the smoothing procedure should distinguish between the two types of contributions. Namely, the divergences that characterize the non-analytic part within an interpolation scheme may be cutoff. There-

fore, the non-analytic part, which is usually known from the theoretical considerations, should be removed prior to smoothing. The remaining short-range contributions are treated separately and separately smoothed using the Fourier interpolation scheme. At the end, now the sort-range contribution define for any momenta and the long-range nonanalytic contribution are added together.

Using this distinction in the treatment of the short-range and the long-range contributions, it is possible to apply Quantum ESPRESSO to calculate the phonon properties and the phonon dispersions. For the cubic zinc-blende boron nitride crystals the corresponding results for the phonon dispersions are shown in Fig. 2. For the hexagonal boron nitride structure, the phonon dispersions are shown in Fig. 3.

II.4. Phonon dispersion for hBN

Besides the cubic zinc-blende BN structure, the hexagonal hBN is another crystalline form of the boron nitride (BN) compound. It has a similar crystalline structure as the graphene, with 2-dimensional monolayers that are bound by van der Waals forces. One unit cell of such crystal is composed of 4 atom, as shown in Fig. 4. The atoms of boron and nitrogen in the same plane are bound by covalent bonds. The bond length is 0.1446 nm, with the nitrogen being slightly more negatively charged than the boron atom. These charges may give rise to long-range interaction. The bonds between the nitrogen and boron atoms in two neighboring layers are of van der Waals nature. The length of these bonds is 0.333 nm. Our results for the phonon dispersion agree well with results obtained in Refs. [7, 10].

In the case of the silicon diamond structure and cubic zinc blende BN structure, we see how two atoms in the unit cell give rises to 6 frequencies. The case of hBN is particularly interesting, because the weak interaction between the monolayers should imply almost a full degeneracy in the spectrum for some of the 12 phonon modes, corresponding to the 4 atoms in the unit cell. As it is expected for the acoustic modes, which are associated to the translation at $\vec{q} = 0$, we find frequencies close to zero for these vibration in the case of the directions $\vec{x}$ and $\vec{y}$ (parallel to the layer plane). There are two frequencies for each of these directions. The first one is characterized by the movement of all atoms in the same direction. The second one, which is a bit higher in energy, is characterized by the movement of atoms in the lower layer in one direction, with atoms in the other layer moving in the opposite direction. For the acoustic modes, in the $\vec{z}$ direction, the translation of both layers together has also a frequency close to the zero value, while the translation of the two layers in opposite directions results with an non-zero value, which may be seen close to the Γ point in Fig. 3, showing the corresponding phonon dispersion for the hBN. These acoustic modes in the $\vec{z}$ direction are characterized by a quadratic contributions near the Γ point as well, rather than an linear one, as in the case for all others acoustic modes.

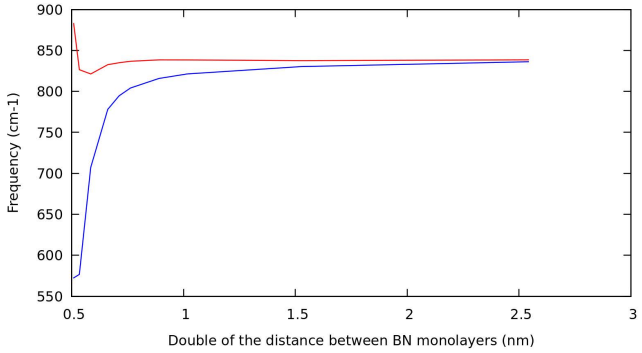

Figure 5. Values of the two optical frequencies for $\vec{q} = 0$ and z direction, as a function of the distance between different layers in hBN. The x axis corresponds to the double of the distance between two BN monolayers as there are two monolayers in one unit cell. The hBN crystal in equilibrium corresponds to the distance of 0.6661 nm between the layers.

From Fig. 4 one observes very different energies of excitations for the optical modes of the hBN crystal at $\vec{q} = 0$. We can see how the $\vec{z}$ vibrations are energetically lower than all the others, which may easily be explained by the weak van der Waals bonds in comparison to the covalent bonds within the layers. The second observation is again an almost negligible difference between the two $\vec{x}$ and $\vec{y}$ vibrations, with the in-phase vibrations being slightly lower in energy than the anti-phase vibrations. The third observation is that the anti-phase vibrations in $\vec{z}$ direction are energetically lower than the in-phase vibrations. Al these details are apparent from the phonon spectrum calculated in Ref. [7] as well.

While the in phase and in anti-phase vibrations in the $\vec{x}$ and $\vec{y}$ directions are almost degenerate and can therefore be only equal for the monolayer optical modes, this is not the case for the vibrations in the $\vec{z}$ direction. We therefore vary the distance between the monolayers in Fig. 5 to show how the both frequencies converge to the value of the monolayer frequency, the latter being equal to the in-phase vibration. This leads to the conclusion that the interaction between the two monolayers in hBN crystal may lower the phonon energy. Furthermore, using the phonon dispersion obtained in Fig. 3, we see that the two $\vec{z}$ frequencies collapse into each other when we are moving into $\vec{z}$ direction.

II.5. Simplified model of macroscopic fields

In order to discuss the appearance of long-range forces in polar crystals we may analyze a simplified model. Let us consider two parallel planes at distance x_0, assuming that the surface charge at one of the plane is equal to σ, whereas at the other the charge is negative σ. These two plates represent a capacitor. The corresponding electric

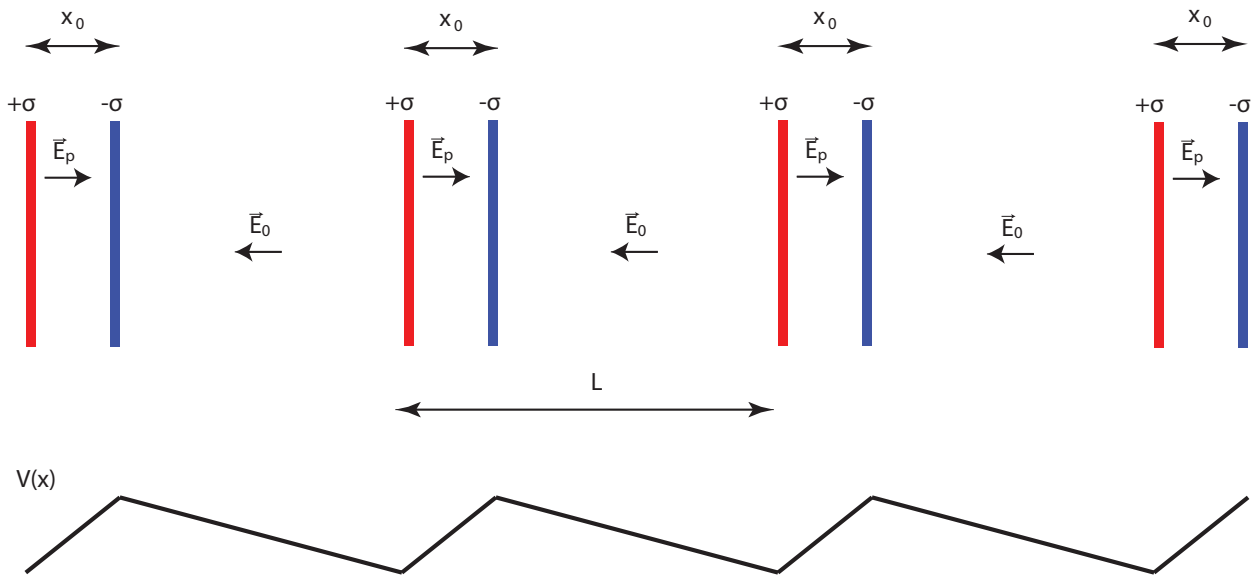

Figure 6. Infinite stack of capacitors, involving infinite charged plates, with an additional electric field E_0 that preserves the periodicity of the electrostatic potential $V(x)$.

field may be found by inspecting the Gauss law. Between plates the field is perpendicular to the planes, $E_p = \sigma$, where ε is the dielectric constant. For infinite planes, outside the capacitor there are no electric fields.

If we now consider an infinite stack of such capacitors repeated periodically with a period L, as in Fig. 6, using the Gauss law it easy to see that the field between capacitors vanishes, whereas the field between plates is the same as for a single capacitor with the surface charge density $\pm\sigma$. In other words, the electrostatic potential $V(x)$ remain constant between capacitors, with drops between plates. To obtain a periodic electrostatic potential the electric field E_0 should be added, as in Fig. 6, in a way that the mean electric field $E_0 + E_p$ over the period L vanishes, $E_0 = -\sigma\, x_0/L$.

If E denotes the mean electric field (macroscopic field) and P denotes the mean polarization, $P = \sigma\, x_0/L$, assuming a linear response, $P = \chi\, E$, we have

$$E = E_0 + E_p = E_0 - 4\pi P \tag{12}$$
$$E_0 = (1 + 4\pi\chi)E \tag{13}$$

where $1 + 4\pi\chi$ corresponds to the dielectric constant ϵ,

$$D = \epsilon E\ . \tag{14}$$

Thus, E_0 in Fig. 6 corresponds to the electric displacement D due to external charges. In other words, the system in Fig. 6 may be described by periodic electrostatic potential of the period L only in the presence of external field. For $D = E_0 = 0$ in Fig. 6, corresponding to LO phonons $q \parallel E, D$, $E = -4\pi P$. Thus, for $D = 0$, the macroscopic electric field E is given by mean polarization. E is antiparallel to P, which means that it effectively enhances the restoring force for the LO phonons.

The present simplified analysis shows the difficulties that appear in the presence of long-range forces in crystals. Because of this forces, one needs to be particularly careful in calculations with boundary conditions at supercell boundaries [3], because the electric polarization averaged over the supercell is nonzero for incommensurate wavelengths. For similar reasons, one needs to be careful with monolayers. Namely, the two-dimensional systems are frequently modeled by repeating periodically layers (planes), while using a large interlayer distance L [11]. However, in the presence of long-range forces, the macroscopic field E, as discussed here, remains finite in the long wavelength limit.

II.6. TO vibrations in hBN

For hBN, we may use a simplified model to explain the different behavior of the dispersion of the two $\vec{z}$ frequencies near the Γ point. These frequencies depend, as one may see from Fig. 7, on the direction of the phonon wave vector. When the phonon wave vector in in the in-plane direction (the case shown on the left side of Fig. 7), the difference in energy of the two $\vec{z}$ modes is significant,. However, in the case when the phonon wave vector is set in the $\vec{z}$ direction (the case shown on the right side of

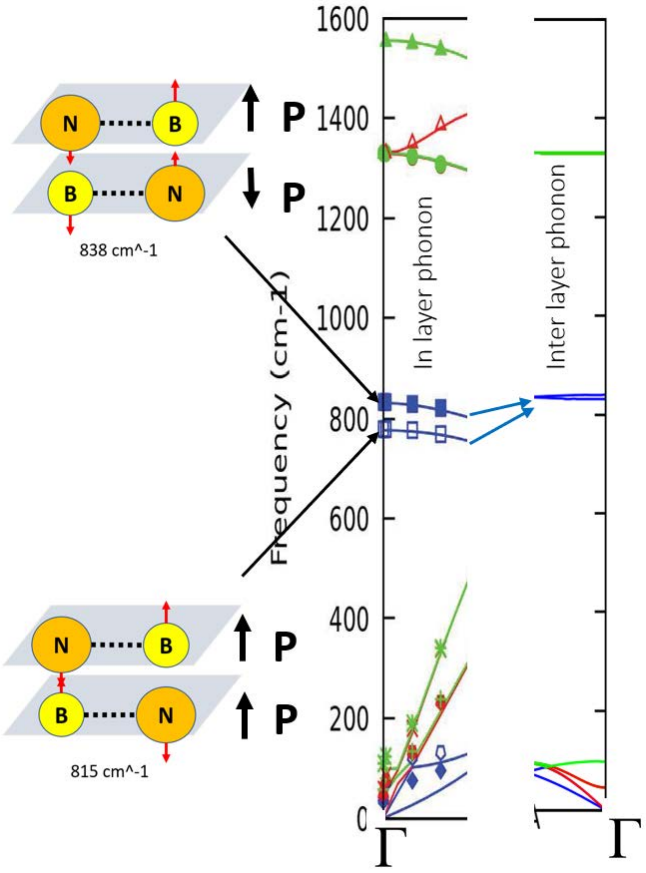

Figure 7. The detailed observation of the different behavior of the dispersion of the phonon in the in-plane or inter-plane direction. We are comparing it directly to the model developed in the previous part.

Fig. 7), the energy difference almost vanishes.

In the first case, we cannot apply the discussed model of capacitors as the phonon waves of the in-layer direction change the polarization only locally but the average of the polarization of one layer stays zero. For this reason, this is the case when there are no macroscopic field created and the calculations for the limit $\vec{q} \to 0$ and $\vec{q} = 0$ give the same value. In the other case, when the phonon wave vector is in the $\vec{z}$ direction, a macroscopic polarization appears. As we can see from Fig. 7, when the two layers oscillate in the antiphase the global macroscopic polarization is again zero, as it is zero in the primitive cell. This explains why there is no change in the energy of the dispersion of this mode when one approaches the Γ point from the in-plane direction or inter plane direction.

This situation is different for the mode involving $\vec{z}$ vibrations that are in phase between the two layers. In this case, there is a macroscopic field when the phonon wave vector is along $\vec{z}$ direction (the LO mode). As a result, the energy of this mode becomes higher. This can explain the difference in energy observed for this mode near the Γ point.

II.7. Comparison with experimental results

While the DFT calculation determines the phonon dispersion in the whole Brillion zone, traditional spectroscopic experiments are limited to the vicinity of the Γ point. These experiments involve the infrared and the Raman spectroscopy, using electromagnetic waves as probes. Because the dispersion of light is given by: $\omega = ck$, where c is the speed of light, excitations of the phonon systems by incident wave involve finite frequencies, while the change of the momentum k is infinitesimally small. This is the reason why these measurements are possible for small $\vec{q}$ of phonons near the Γ point. Nevertheless, this is fully sufficient to observe the LO/TO splitting effect.

In the case of the infrared spectroscopy, one measures the spectrum of photon absorptions in the interval of frequencies that is of the same order as the phonon frequencies. The absorption of the incident photon is a result of an excitation of a phonon of the same wave vector k and frequency ω. On the other hand, the Raman scattering uses phonon of high frequencies and measures their inelastic scattering with the optical phonons. That is, we measure the Raman shift between the incident and the

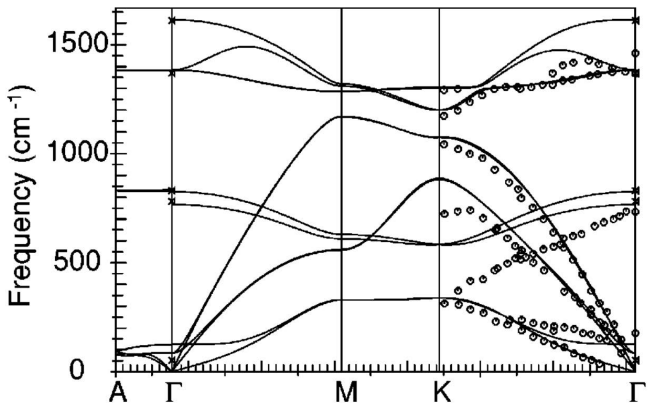

Figure 8. Phonon-dispersion relations of h-BN [7]. The full curves show the results of the ab initio force-constant approach. The symbols at Γ point indicate the Raman and the infrared data. The open circles represent the HREELS data for a monolayer of h-BN on the Ni 111 substrate.

transmitted wave, which in return corresponds to the frequency of the phonon with which the light interacts.

If a unit cell has a center of symmetry, depending on the symmetry of the lattice vibrations, the phonons may be infrared active or/and Raman active. In the case of infrared active phonons, the absorption of the photon induces a dipole momentum. Thus, the corresponding lattice displacements should involve the dipole momentum for the phonon excitation to be possible. This implies that the positive and the negative charges move in opposite directions. In the Raman case, it is the polarizability that should change. The Raman active modes may be induced by a displacements of only positive or negative charges move symmetrically. In this way, the infrared and Raman spectroscopy are complementary and we need to use both of them to obtain the energies of all phonon modes around the Γ point.

As always, it is particularly important to check the calculations by comparing to available experimental data. In particular, we may compare our DFT calculations with the spectra published in Ref. [7] for hBN. The results are shown on Fig. 8. We may clearly see the agreement of the DFT calculations with the spectroscopic measurements near the Γ point. In addition, the third kind of measurements using HREELS, shown in Fig. 8, provides a larger part of the dispersion between Γ and K points. These measurements are special, involving a highly collimated monochromatic electron source with a very narrow energy distribution. In this way the problem of the extremely sharp photon dispersion is lifted, using electrons as probes instead of photons. The limitation of HREELS is that it may be applied for 2D materials in certain crystal directions only. Nevertheless, from Fig. 8 we observe again a surprisingly good agreement with the DFT calculations, now beyond the proximity of the Γ point.

III. CONCLUSIONS

The lattice properties of silicon and boron nitride crystals are analyzed. In the case of the latter, two structures are discussed, the first is in the cubic zinc-blende structure, which is diamond like an similar to the silicon. The second is hexagonal graphite like, hBN, with weak van der Waals bonds between layers. The first task in modeling the crystal structure is to find the equilibrium lattice coordinates, corresponding to the minimal energy of the crystal. The vibrations around this equilibrium configuration correspond to the phonon modes, that we calculated using Quantum ESPRESSO software package. Using this approach, phonon spectra involving different acoustic and optical phonon modes are obtained, for transverse and longitudinal polarization. Unlike for silicon crystals, the spiting between TO and LO modes is found for BN crystals. This spiting is caused by different charges at B and N atoms, which are source of long-range force. It is argued that in the case of the LO phonon displacements a macroscopical polarization develops, corresponding to an electrical field that enhances the restoring force for vibrations. This explains why the LO modes are higher in energies than the TO modes. Furthermore, it is argued here that the long-range force represent a separate problem for the phonon calculations, and should be treated separately from the short-range force, well capture by standard approaches to the dynamical matrix. Out calculated spectra show a very god agreement with the results in the literature, with many details discussed separately. It may be concluded that the numerical approaches and software packages like Quantum ESPRESSO, when appropriately used, represent a power tool for calculating the crystal structure and the phonon spectra, even in the presence of long-range forces.

[1] NSM Archive - Physical Properties of Semiconductors
[2] X. Gonze, C. Lee, Dynamical matrices, Born effective charges, dielectric permittivity tensors, and interatomic force constants from density-functional perturbation theory, Phys. Rev. B **55**, 10355 (1997).
[3] Yi Wang, Shun-Li Shang , Huazhi Fang , Zi-Kui Liu and Long-Qing Chen, First-principles calculations of lattice dynamics and thermal properties of polar solids, npj Comput. Mater. **2**, 16006 (2016).
[4] P. Giannozzi, S. De Gironcoli, P. Pavone, S. Baroni, S. D. Gironcoli, P. Pavone, S. Baroni, S. De Gironcoli, P. Pavone, and S. Baroni, Ab initio calculation of phonon dispersions in semiconductors, Phys. Rev. B **43**, 7231 (1991).
[5] S. Baroni, S. De Gironcoli, A. Dal Corso, and P. Giannozzi, Phonons and related crystal properties from density-functional perturbation theory, Rev. Mod. Phys. **73**, 515 (2001), arXiv:0012092v1.

[6] X. Gonze, J.-C. Charlier, D. C. Allan, and M. P. Teter, Interatomic force constants from first principles: The case of α-quartz, Phys. Rev. B **50**, 13035 (1994).

[7] G. Kern, G. Kresse, and J. Hafner, Ab initio calculation of the lattice dynamics and phase diagram of boron nitride, Phys. Rev. B **59**, 8551 (1999).

[8] R. Tubino, L Piseri, and G Zerbi, Lattice Dynamics and Spectroscopic Properties by a Valence Force Potential of Diamondlike Crystals: C, Si, Ge, and Sn, J. Chem. Phys. **56**, 1022 (1972).

[9] M. Kazan, G. Guisbiers, S. Pereira, M. R. Correia, P. Masri, A. Bruyant, S. Volz, and P. Royer, Thermal conductivity of silicon bulk and nanowires: Effects of isotopic composition, phonon confinement, and surface roughness, J. Appl. Phys. **107**, 083503 (2010).

[10] K. H. Michel and B. Verberck, Phonon dispersions and piezoelectricity in bulk and multilayers of hexagonal boron nitride, Phys. Rev. B **83** 115328 (2011).

[11] T. Sohier, M. Gibertini, M. Calandra, F. Mauri, N. Marzari, Breakdown of Optical Phonons Splitting in Two-Dimensional Materials, Nano Lett. **17**, 3758 (2017).